Science Advances

AAAS

advances.sciencemag.org/cgi/content/full/3/11/e1700807/DC1

Supplementary Materials for

Adaptability as the key to success for the ubiquitous marine nitrite oxidizer *Nitrococcus*

Jessika Füssel, Sebastian Lücker, Pelin Yilmaz, Boris Nowka, Maartje A. H. J. van Kessel, Patric Bourceau, Philipp F. Hach, Sten Littmann, Jasmine Berg, Eva Spieck, Holger Daims, Marcel M. M. Kuypers, Phyllis Lam

Published 1 November 2017, *Sci. Adv.* **3**, e1700807 (2017)
DOI: 10.1126/sciadv.1700807

The PDF file includes:

Other Supplementary Material for this manuscript includes the following:
(available at advances.sciencemag.org/cgi/content/full/3/11/e1700807/DC1)

- table S1 (Microsof Excel format). Percent identity of 16*S* rRNA genes between *N .mobilis* and the newly identified *Nitrococcus*-like phylotype 1.
- table S2 (Microsof Excel format). List of marine environmental metagenomes that contain at least one of the four *Nitrococcus* phylotypes.
- table S3 (Microsof Excel format). List of marine amplicon sequencing data sets that contain at least one of the four *Nitrococcus* phylotypes.

- table S4 (Microsof word format). *N. mobilis* strain Nb-231 proteins with predicted functions in key metabolic pathways.
- table S5 (Microsof Excel format). ^{13}C enrichment of single *Nitrococcus* cells from the Namibian OMZ.
- table S6 (Microsof Excel format). Composition of marine NOB medium used to grow *N. mobilis.*
- table S7 (Microsof Excel format). Functional genes associated with *Nitrococcus* spp. in selected Tara Oceans metagenomes.
- table S8 (Microsof Excel format). Summary of stations, sampling depths, and ^{15}N incubation experiments conducted.
- table S9 (Microsof Excel format). NOB specific 16*S* rRNA-targeted oligonucleotide probes.
- table S10 (Microsof Excel format). Substrate amendments for *N. mobilis* Nb-231 incubation experiments.

Supplementary Text

Assessment on Anaerobic Nitrite Oxidation Potential

While anaerobic oxidation of nitrite by Fe(III) and Mn(IV) is thermodynamically feasible, their low abundance in the water column [*64*] render them unlikely candidates as electron acceptors in pelagic environments. Chlorate (ClO_3^-) is known to serve as alternative electron acceptor in nitrite oxidation, the reaction product chlorite, however, efficiently inhibits NOB [*65*] and ClO_3^- rarely occurs naturally. Iodate (IO_3^-) is a structural analog of chlorate and the anaerobic oxidation of NO_2^- with IO_3^- would be thermodynamically feasible ($3NO_2^- + IO_3^- \rightarrow 3NO_3^- + I^-$; $\Delta G_0' =$ -48.6 kJ/mol). Concentrations of IO_3^- in seawater range between 0.1-0.6 µM and in anoxic basins IO_3^- appears to be biologically reduced to iodide (I^-) resulting in subsurface I^- maxima [*66–68*].

To investigate the potential for nitrite oxidation with IO_3^-, degassed environmental samples from the Namibian OMZ were amended with IO_3^-. In samples from the lower OMZ (O_2 < 20 µM) NO_2^- oxidation rates increased significantly ($p<0.05$; Wilcoxon matched pairs test; fig. S7), potentially indicating the utilization of IO_3^- by NOB. A similar pattern was however also observed in the absence of IO_3^- when samples were solely purged with helium prior to incubation ($p<0.05$; Wilcoxon matched pairs test; fig. S7). Thus, when the ambient O_2 concentrations were low (<20 µM), the reduction of oxygen in the incubation vessels enhanced nitrite oxidation. Oxygen contaminations inevitably occur during sampling with a CTD rosette and appear to inhibit NOB from the lower OMZ. Hence, these results imply the activity of highly adapted microaerophilic NOB in the lower OMZ. Since IO_3^- addition and reduction of oxygen concentrations had the same enhancing effect on nitrite oxidation, the utilization of IO_3^- as electron acceptor was not confirmed.

Anaerobic oxidation of nitrite could alternatively be facilitated via nitrite disproportionation to N_2 and NO_3^- ($5\ NO_2^- + 2H^+ \rightarrow N_2 + 3\ NO_3^- + H_2O$; $\Delta G' =$ -68.6 kJ/mol). The different reaction stoichiometries of nitrite disproportionation and canonical denitrification ($2\ NO_2^- + 10\ e^- + 8\ H^+ \rightarrow N_2 + 4\ H_2O$) would allow the differentiation of the processes in ^{15}N labeling experiments. In our incubation experiments 11 to 600 times more $^{15}NO_3^-$ was produced than $^{29}N_2$, with the exception of one bottom water sample that exhibited a 1:1 ratio of both products. Production of $^{30}N_2$ could not be detected. Thus, neither nitrite disproportionation nor canonical denitrification

appears to contribute to N_2 production in the Namibian OMZ. The parallel occurrence of aerobic or anaerobic nitrite oxidation and nitrite disproportionation however would increase the ratio of $^{15}NO_3^-$ over $^{29}N_2$ and based on the current data we cannot exclude the occurrence of nitrite disproportionation.

Genomic analysis

The sequence deposited at GenBank consists of 43 assembled contigs. The draft genome has a size of 3,617,638 bases and contains 3552 open reading frames (ORFs) encoding for 3503 protein coding genes (coding sequence, CDS), one complete rRNA operon, and 45 tRNA genes for all 20 amino acids, between 1 and 5 for each tRNA type. The average GC content is 59.97%.

Nitrogen uptake

For transport of nitrite into the cytoplasm, *N. mobilis* Nb-231 encodes three transporters, one NirC-type nitrite importer, and two NarK-type nitrate/nitrite transporters that function as antiporters and simultaneously export nitrate. Nitrogen assimilation is facilitated by a NirBD-type nitrite reductase and by direct uptake of ammonium by an Amt-type ammonium transporter (Fig. 2). Further, a cyanase might also supply the cell with ammonium, most likely as side effect of cyanate detoxification [*69*]. No assimilatory nitrate reductase could be identified in the *N. mobilis* Nb-231 genome, but this function will be performed by NXR in the absence of nitrite

Nitrite oxidoreductase of Nitrococcus

In NOB, the central enzyme complex for energy conservation during aerobic chemolithoautotrophic growth with nitrite and carbon dioxide as sole energy and carbon sources, respectively, is the nitrite oxidoreductase system (NXR). NXR belongs to the type II group in the dimethyl sulfoxide reductase family of molybdopterin-cofactor-binding enzymes [*70*], also referred to as complex iron-sulfur molybdoenzyme (CISM) family [*71*] or more recently as the Mo/W-*bis*PGD enzymes family [*72*]. These oxidoreductase systems typically consist of three subunits, a catalytic alpha subunit containing the molybdenum *bis* molybdopterin guanine dinucleotide (Mo-*bis*-MGD) cofactor and one [4Fe–4S] iron-sulfur (Fe-S) cluster, an electron-transporting beta subunit with one [3Fe-4S] and three [4Fe-4S] clusters which shuttles the electrons between the alpha and the usually membrane-integral gamma subunit. The gamma subunit functions as membrane anchor for the holoenzyme and transfers the electrons to and from the electron transport chain via one or two haems [*71*], but a lot of variations to this theme exist

[*72*]. The genome of *Nitrococcus mobilis Nb*-231 contains one genomic region encoding all three structural NXR genes as well as the delta subunit, which functions as chaperone in inserting the molybdenum cofactor into the alpha subunit [*73*]. The NXR of *N. mobilis* Nb-231 is most similar to the enzyme systems found in *Nitrobacter* and *Nitrolancea*, as well as to the nitrate reductase system of *Candidatus* Methylomirabilis oxyfera [*14*, *27*, *29*]. The gene order in all these organisms is highly conserved and includes besides the NXR alpha, beta, delta, and gamma (*nxrABDC*) subunits also a gene for a cytochrome *c*-like protein with binding patterns for two haems *c* upstream of *nxrA* [*29*]. As electrons derived from nitrite oxidation enter the respiratory chain at the level of cytochrome *c*, this dihaem protein likely serves as primary electron acceptor for NXR.

The subunits of NXR do not contain signal peptides for protein secretion, thus indicating a cytoplasmic orientation of the enzyme as was described for *Nitrobacter* and *Nitrolancea hollandica* [*28*, *29*]. In contrast, *Nitrospina* the active subunit of NXR is localized on the periplasmic side of the cytoplasmic membrane, which indicates that the net release of two scalar protons during nitrite oxidation can directly contribute to proton motive force (PMF) generation [*14*, *27*]. A cytoplasmic orientation in contrast implies lower energy yield, as the protons from nitrite oxidation do not contribute to PMF. In other words, while *Nitrospina* appears to efficiently utilize even low amounts of nitrite, *Nitrococcus* is likely inefficient under substrate-limited conditions.

Carbon dioxide fixation

Carbon dioxide fixation in *N. mobilis* Nb-231 is carried out by the Calvin-Benson-Bassham (CBB) cycle. The large and small subunits of the key enzyme ribulose bisphosphate carboxylase/oxygenase (RubisCO) are encoded in the genome, as are the phosphoribulokinase and all other enzymes involved in the CBB cycle. The RuBisCO is of the green form I and most similar to its homologs in *Cyanobacteria*, but also to one of the RuBisCO paralogs in *Nitrobacter* and *Nitrosomonas* [*29*]. The genome encodes a second RuBisCo-like protein, but this copy is of the type IV which has been shown to be involved in the methionine salvage pathway [*74*]. Genome annotation further revealed all genes necessary for carboxysome formation, which is a common mechanism for concentrating CO_2 in organisms using the CBB cycle [*75*]. Genes for glycolate salvage and the glyoxylate shunt of the tricarboxylic acid (TCA) cycle are also present

and allow metabolizing the phosphoglycolate byproduct that is formed when RuBisCO reacts with O_2 at low CO_2 concentrations [*76*]. Furthermore, a phosphoenolpyruvate carboxylase replenishes oxaloacetate in the TCA cycle.

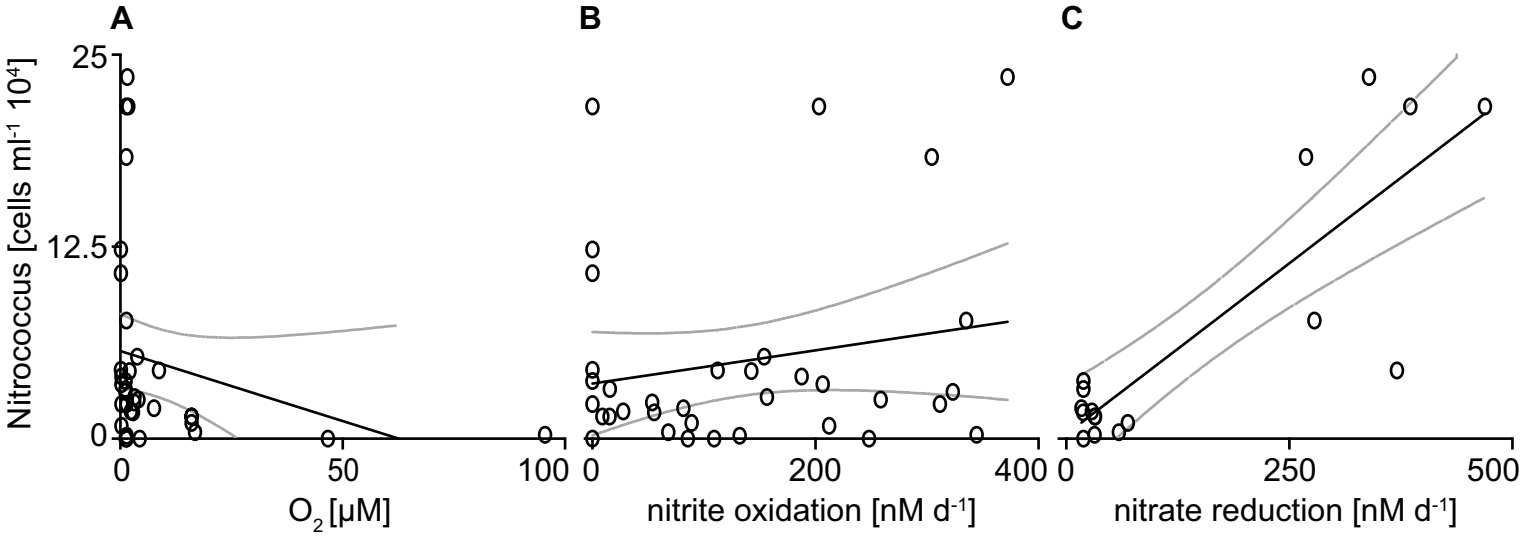

fig. S1. Abundance of *Nitrococcus*-affiliated cells in the Namibian OMZ based on CARD-FISH counts. Abundance of Nitrococcus-affiliated cells in the Namibian OMZ based on CARD-FISH counts related to (A) ambient O_2 concentrations (R^2: 0.06; p-value > 0.2), (B) to nitrite oxidation rates (R^2: 0.04; p-value: 0.3), and (C) to nitrate reduction rates (R^2: 0.7; p-value <0.0001). Data points are shown as open circles with the corresponding linear regression (black lines) and the 95% confidence interval (grey lines), values for R^2 and p are derived from linear regression analysis.

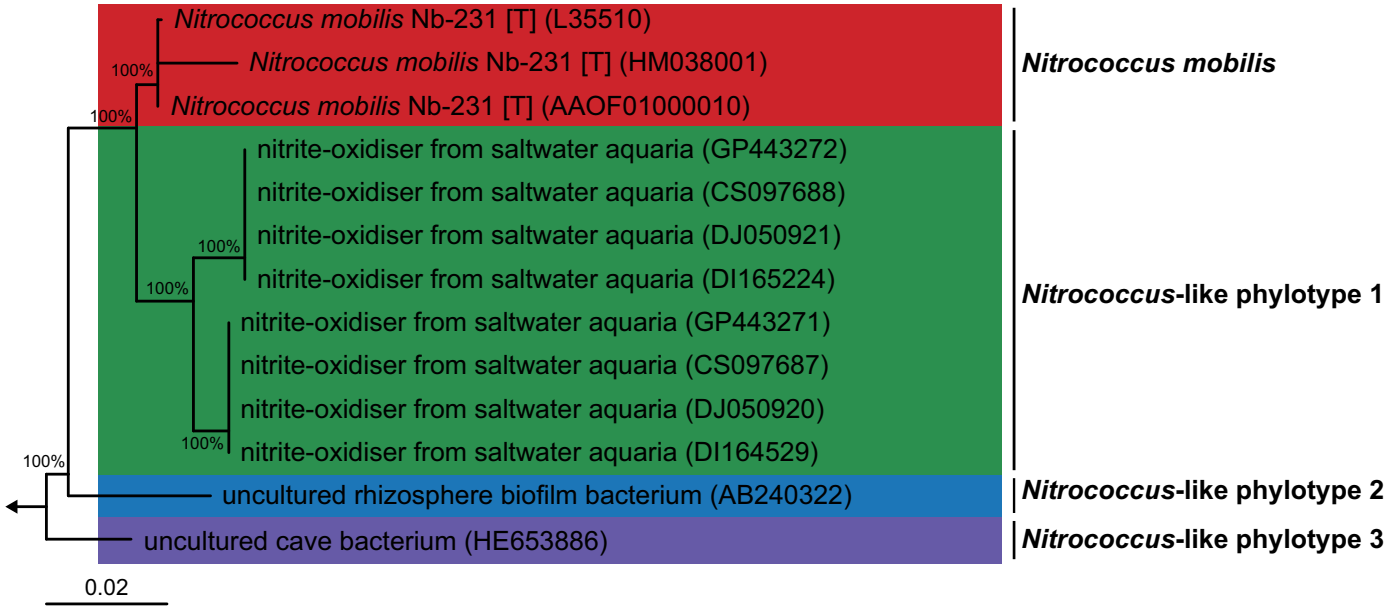

fig. S2. 16*S* rRNA gene-based phylogenetic tree visualizing the relation of four *Nitrococcus* phylotypes. 16S rRNA gene-based phylogenetic tree visualizing the relation of four *Nitrococcus* phylotypes that were also detected within the available metagenomic and 16S rRNA amplicon datasets. *Arhodomonas aquaeolei* served as outgroup (indicated with the arrow), and bootstrap values are shown only when they were above 60%. The bar indicates 0.02 substitutions per nucleotide position. Nucleotide sequence accession numbers are indicated in parentheses.

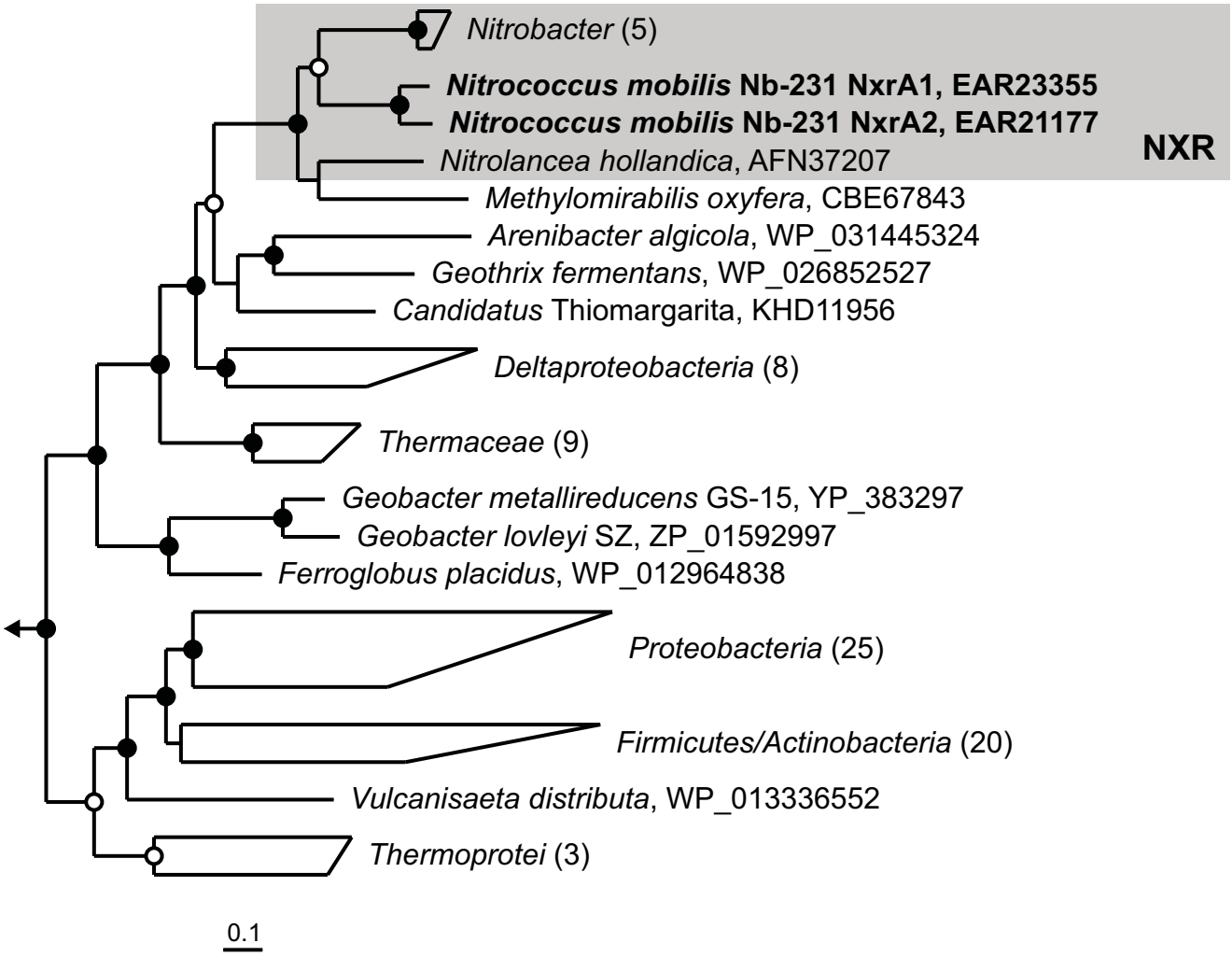

fig. S3. Phylogenetic analysis of NxrA. Maximum-likelihood tree showing the affiliation of the two *N. mobilis* Nb-231 NxrA copies within the nitrate reductase (NarG) sequence group of the type II DMSO reductase family. The grey box highlights the known nitrite-oxidizing bacteria. Numbers in brackets indicate sequences per group. Bootstrap support ≥70% and ≥90% is indicated by open and filled circles, respectively. The arrow indicates the position of the outgroup. The scale bar corresponds to 10% sequence divergence. NXR, nitrite oxidoreductase.

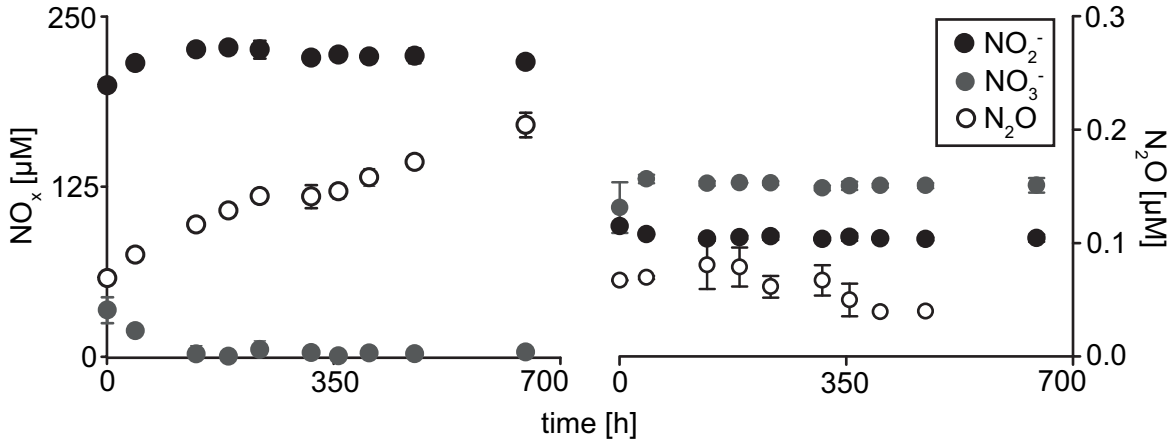

fig. S4. Incubation experiments with *N. mobilis* Nb-231. Pure cultures were incubated under anaerobic conditions in seawater medium containing 200 µM $^{15}NO_2^-$ and 80 µM IO_3^- (left panel). A control experiment with autoclaved cultures of *N. mobilis Nb-231* was conducted under identical conditions (right panel). Concentrations of NO_2^- (black circles), NO_3^- (grey circles) and N_2O (open circles) were measured over a time course of 700 h.

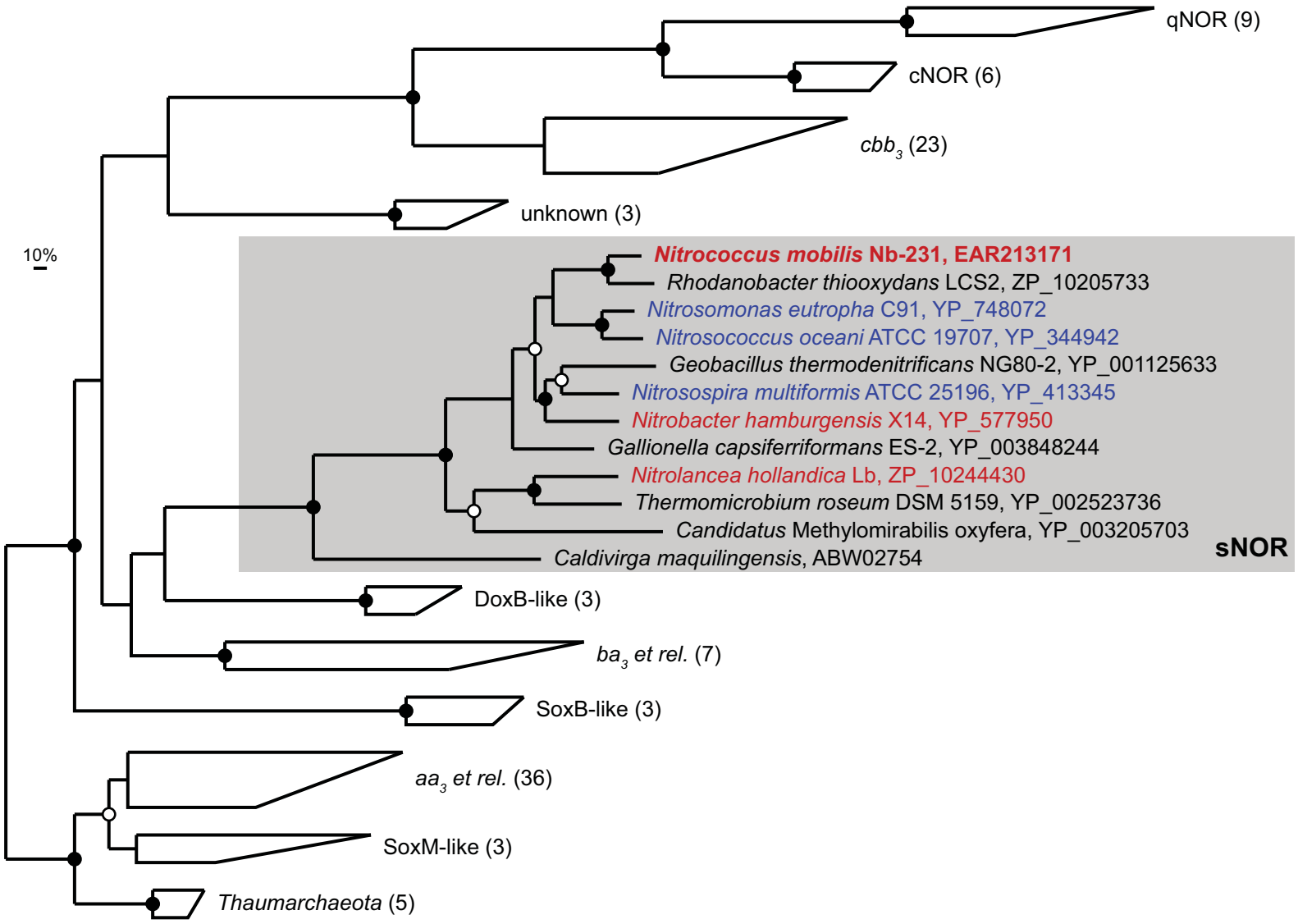

fig. S5. Phylogenetic analysis of the sNOR. Maximum-likelihood tree showing the affiliation of the *N. mobilis* Nb-231 putative NO reductase within the heme-copper oxidase family. The grey box highlights the putative sNOR family. Red denotes nitrite-oxidizing and blue ammonia-oxidizing bacteria. Numbers in brackets indicate sequences per group. Bootstrap support ≥70% and ≥90% is indicated by open and filled circles, respectively. The arrow indicates the position of the outgroup. The scale bar corresponds to 10% sequence divergence.

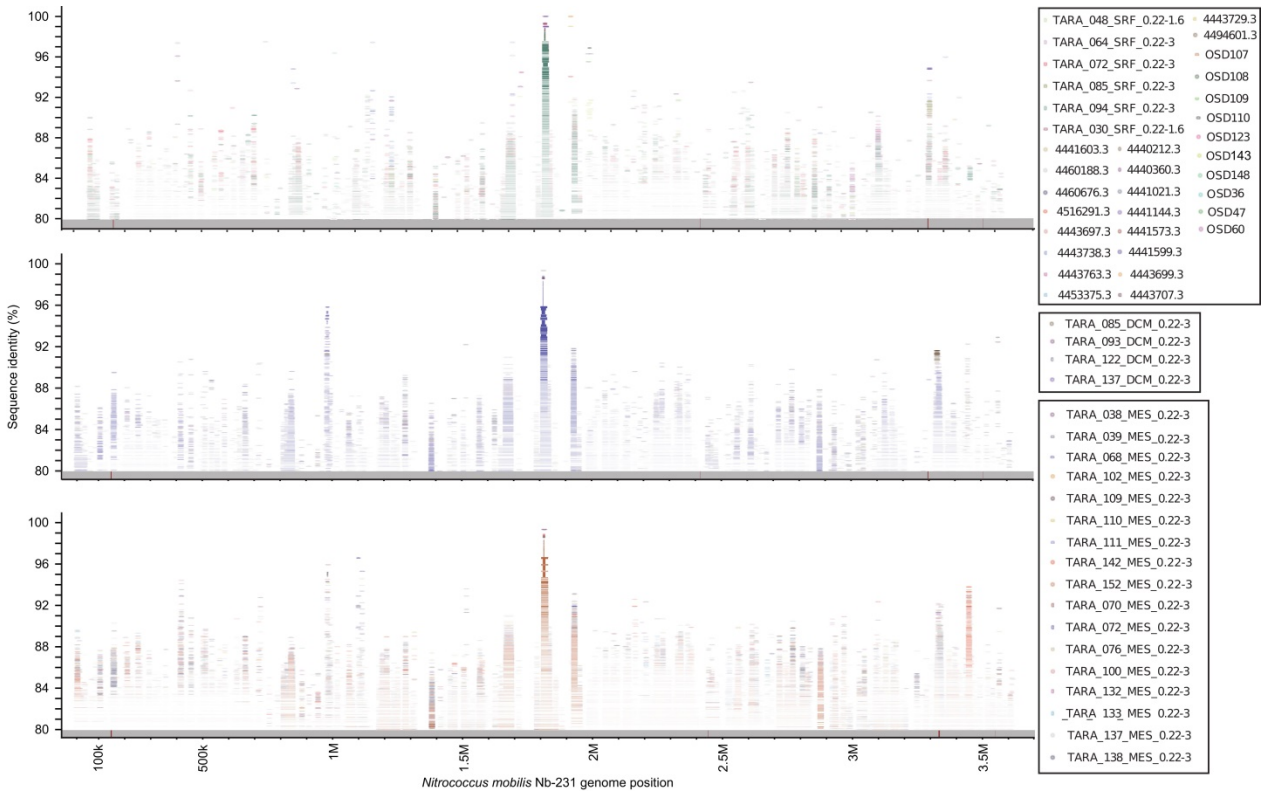

fig. S6. Selection of Tara Oceans, MG-RAST, and OSD samples that were mapped to the *N. mobilis* Nb-231 genome. Samples from surface waters **(A)**, the deep chlorophyll maximum (DCM) **(B)** and mesopelagic waters **(C)** were analyzed. Functional genes from left to right are indicated by vertical bars on the x-axis, line thickness is relative to gene length: Nitrite oxidoreductase 2 (*nxrA2*, 146722 to 150384), Sulfide:quinone oxidoreductase (*sqr*, 2443855 to 2445099), Sulfite dehydrogenase subunit A (*sorA*, 2902992 to 2904233), Nitrite oxidoreductase 1 (*nxrAB*, 3330859 to 3334515) and Putative NO reductase complex (sNOR, 3550084 to 3550680).

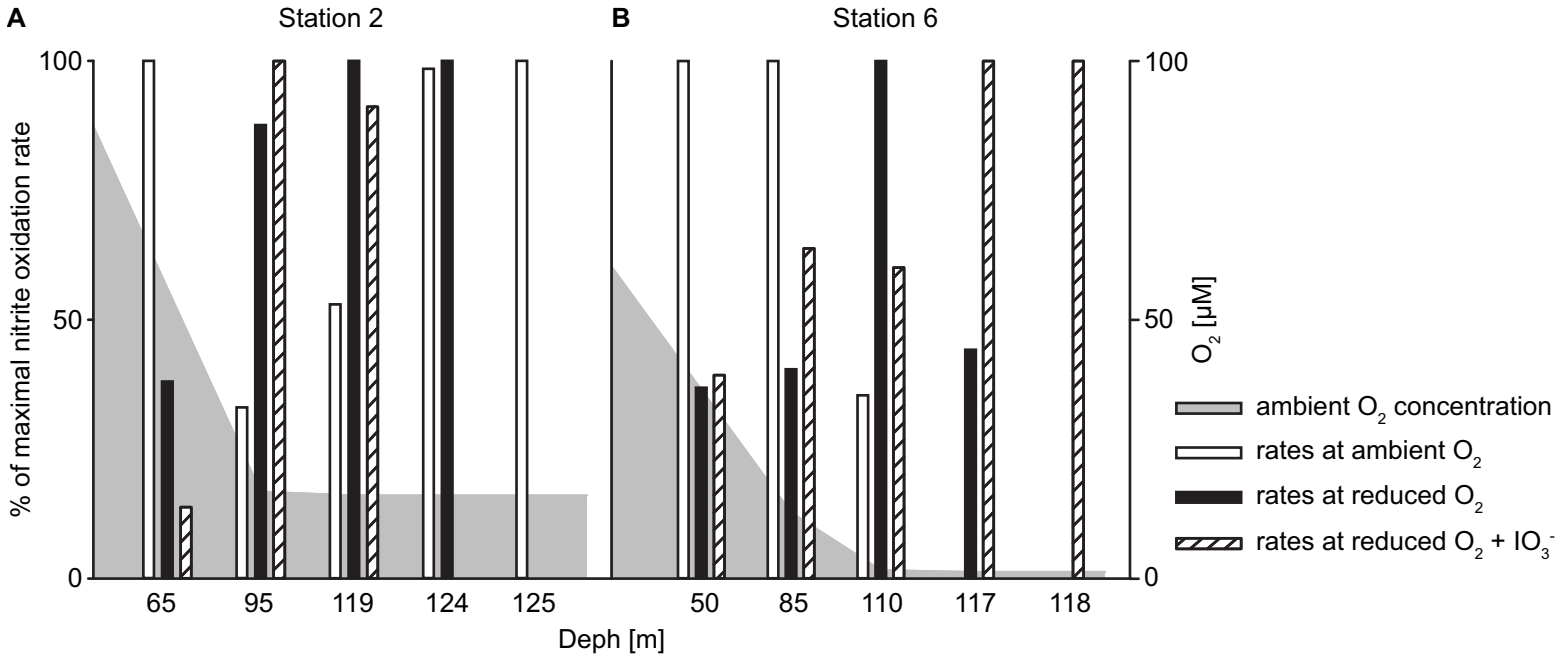

fig. S7. Effect of reduced O_2 and enhanced IO_3 concentrations on nitrite oxidation rates. Rates of nitrite oxidation (vertical bars) measured as the production of $^{15}NO_3^-$ from $^{15}NO_2^-$ over time at two stations in the Namibian OMZ including 5 depths. Samples were incubated under ambient O_2 (white bars), reduced O_2 (black bars) and reduced O_2 concentrations plus IO_3^-(striped bars). Maximal nitrite oxidation rates measured at each depth was set to 100%. Rates measured under different incubation conditions are depicted as proportions of the maximal rate observed. Ambient oxygen concentrations at the sampling depths are indicated by in gray.